Photo- and Electrochemical Properties of a CO2 Reducing Ruthenium–Rhenium Quaterpyridine-Based Catalyst

Frayne, L.; Das, N.; Paul, A.; Amirjalayer, S.; Buma, W.J.; Woutersen, S.; Long, C.; Vos, J.G.; Pryce, M.T.

DOI
10.1002/cptc.201700197

Publication date
2018

Document Version
Final published version

Published in
ChemPhotoChem

ChemPubSoc Europe

DOI: 10.1002/cptc.201700197

CHEMPHOTOCHEM Articles

Special Issue

Photo- and Electrochemical Properties of a CO_2 Reducing Ruthenium–Rhenium Quaterpyridine-Based Catalyst

Liam Frayne,[a] Nivedita Das,[a] Avishek Paul,[a] Saeed Amirjalayer,[c] Wybren J. Buma,[b] Sander Woutersen,[b] Conor Long,[a] Johannes G. Vos,[a] and Mary T. Pryce*[a]

The bridging ligand 2,2′,5′,3″,6″,2‴-quaterpyridine was utilised to tether $[(bpy)_2Ru]^{2+}$ and $[Re(CO)_3Cl]$ subunits for the purpose of photocatalytic CO_2 reduction. The photophysics and electrochemistry of the complex and associated mononuclear species are reported herein, in addition to photocatalytic, picosecond time-resolved infrared and computational studies. Photophysical, time-resolved IR, and electrochemical data together with quantum chemical calculations indicate weak communication between the two metal centres. As a result of the electron-withdrawing effect of the ligand on both the Ru and Re subunits, the reducing power of the photosensitiser and catalytic unit were significantly attenuated relative to the intermolecular approach utilising $[(bpy)_3Ru]^{2+}$ and $(bpy)Re(CO)_3Cl$.

1. Introduction

CO_2 levels in the atmosphere have continually increased[1] since the industrial revolution, with levels now greater than 400 ppm. There is an urgent need to develop CO_2 reduction technologies, as no single approach is capable of reducing CO_2 levels in the atmosphere. Therefore to achieve this, many technologies must be developed. At present, renewable sources such as wind, tidal, hydroelectric and solar energy focus on energy harnessing, but its storage is more problematic. Of particular interest is the development of photocatalytic CO_2 reduction, a technique that is aimed at the storage of high energy molecular components such as CO and formic acid. An efficient molecular photocatalytic assembly for CO_2 reduction requires the use of a photosensitiser that can absorb light in the visible region and transfer the electron to the catalytic centre. Both inter- and intramolecular approaches of photocatalytic systems have been explored. For intramolecular photocatalysts the selection of an appropriate bridging ligand is of utmost importance, as it should allow electron transfer from the photosensitiser to the catalyst but at the same time limit the electronic interaction between the two moieties.

Intramolecular systems have been studied, with a view to visible light driven catalytic CO_2 reduction. These systems have predominantly used (bipyridine)$Re(CO)_3(X)$ as the catalytic centre because of its stability. Ishitani and co-workers have studied a wide range of supramolecular assemblies linking Re–Ru units,[2–4] and with a view to improving these intramolecular systems for CO_2 photocatalysis, a host of parameters have been varied. These include the use of both conjugated/non-conjugated bridges, the addition of substituents on the bridging ligand and peripheral ligands of both metal centres, and increasing the numbers of photosensitising/catalytic centres within the molecules. The best performance in terms of the amount of CO detected was reported for non-conjugated bridging units. The turn over numbers (TONs) for CO generation in these studies ranged from 10 to greater than 3000, as either the bridge or peripheral groups were varied.[5–11] Thus far, Ru–Re and Ru–Ru approaches appear to be the most promising. The highest homogeneous TON_{CO} and TON_{HCOOH} achieved were 3029 and 2766 for a Ru–Re[6] and Ru–Ru[12] complex.[3] With the utilisation of TEOA as a sacrificial donor, a Zn porphyrin–Re approach achieved 332 TON_{CO}.[13] However, aside from Ru–Re, Ru–Ru, Ir–Re, Os–Re, Ir–Ir and Re–Zn porphyrins, TON values for CO are relatively low. A very recent review by Fontecave and co-workers, comprehensively describes a wide range of molecular catalysts for CO_2 reduction.[14]

In this contribution, we report on the synthesis, photophysical properties, time-resolved IR (TRIR) spectroscopy, quantum chemical calculations, and electrochemical characterisation of the complexes shown in Figure 1. Their capacity for the light-driven reduction of CO_2 was also investigated. In these studies, we explore the photo-activity of the intramolecular compound RuRe (**5**) for CO_2 reduction and compare the results obtained with those of the intermolecular approach with mixtures containing the mononuclear complexes $[(bpy)_3Ru]^{2+}$ (**1**) and

[a] Dr. L. Frayne, Dr. N. Das, Dr. A. Paul, Prof. Dr. C. Long, Prof. Dr. J. G. Vos, Dr. M. T. Pryce
School of Chemical Sciences
Dublin City University
Glasnevin, Dublin 9, Ireland
E-mail: mary.pryce@dcu.ie
[b] Prof. Dr. W. J. Buma, Prof. S. Woutersen
Van't Hoff Institute for Molecular Sciences
University of Amsterdam
Science Park 904, 1098 XH, Amsterdam, 1090 GD, Amsterdam, The Netherlands
[c] Dr. S. Amirjalayer
Physikalisches Institut
Westfälische Wilhelms-Universität Münster
Willhelm-Klemm-Strasse 10, 48149 Münster (Germany)
and
Center for Nanotechnology (CeNTech)
Heisenbergstrasse 11, 48149 Münster (Germany)

Supporting information for this article is available on the WWW under https://doi.org/10.1002/cptc.201700197

An invited contribution to a Special Issue on Artificial Photosynthesis

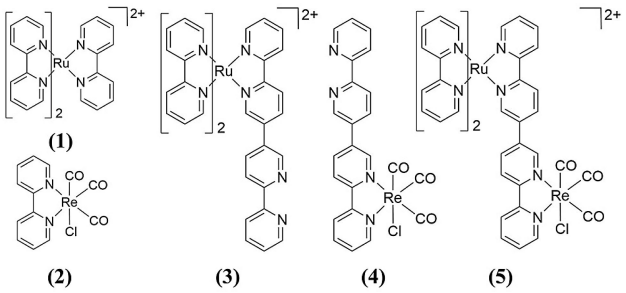

Figure 1. Structures of the quaterpyridine and bipyridine Ru and Re complexes studied.

(bpy)Re(CO)$_3$Cl (**2**). The effect of the solvents and the sacrificial agents used are also addressed.[15–17] To the best of our knowledge, a quaterpyridine (qpy) bridging ligand has not previously been utilised towards intramolecular photocatalytic CO_2 reduction.[18]

2. Results and Discussion

2.1. Synthesis

The synthesis of the mononuclear Ru-quaterpyridine complex (**3**) and the quaterpyridine ligand has been reported elsewhere.[19] The rhenium complex (**4**) was synthesised under an Ar atmosphere, through the slow addition of Re(CO)$_5$Cl to 2,2′:5′,3″:6″,2‴-quaterpyridine in toluene at reflux temperature. The Ru–Re dinuclear complex (**5**) was synthesised by the addition of Re(CO)$_5$Cl to an ethanol solution containing the mononuclear Ru-quaterpyridine complex (**3**). Further details regarding synthesis are contained in the experimental section.

2.2. Spectroscopic Properties

2.2.1. ^{1}H NMR Spectroscopy

The ^{1}H NMR and COSY spectra of all the compounds are included in the Supporting Information (Figures S1–8). The assignments for the protons in these spectra are in agreement with those of other related compounds.[19] Further details on the assignments are available within the experimental section. (NOTE that an NMR spectrum of the deuterated compound (**3**) is included in the Supporting Information NMR section)

2.2.2. UV/Vis Absorption Spectroscopy

The absorption and emission data of the complexes are presented in Table 1 and shown in Figure 2.

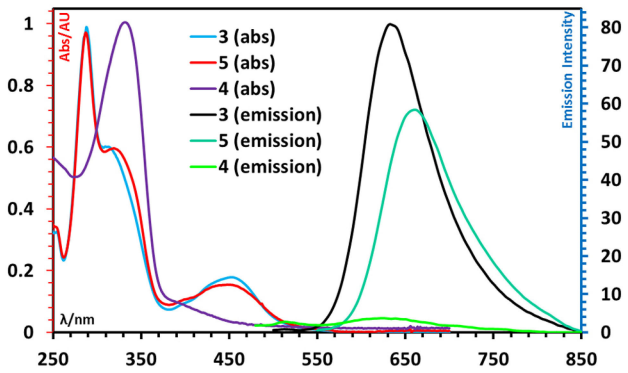

Figure 2. Absorption and emission spectra (λ_{exc} = 450 nm) of compounds **3** (10^{-5} M for absorbance), **4** (10^{-4} M for absorbance) and **5** (10^{-5} M for absorbance) recorded in acetonitrile. For the emission spectra, the ODs at λ_{exc} = 450 nm were 0.17, 0.15 and 0.16 A.U., respectively

The mononuclear rhenium complex **(4)** has an absorption band at 335 nm with a shoulder tailing to 500 nm. The former is assigned to a π-π* transition of the quaterpyridine ligand and the lower energy feature is attributed to a ^{1}MLCT transition from rhenium to quaterpyridine.[20–22] In the case of the dinuclear complex (**5**), spectral features with λ_{max} at 450, 323 and 287 nm are apparent. The feature with a λ_{max} at 450 nm is assigned to a ^{1}MLCT and is expected to contain a contribution from both Ru→bipyridine and Ru→quaterpyridine based on the literature.[19,23,24] Our calculations, as discussed later, suggest that this transition is mainly Ru→bipyridine charge transfer in character. The absorption band at 323 nm is attributed to quaterpyridine ligand centred π-π* transitions, based on similarities with complexes **3** and **4**. With reference to complexes **1**,[25] **3** and to other Ru–Re assemblies,[5,23] the feature with λ_{max} of 287 nm is attributed to bipyridine ligand-centred π-π* transitions. The Re→quaterpyridine ^{1}MLCT is not easily attributable within compound **5**. Previously reported Ru–Re systems have however shown that the Re→ligand ^{1}MLCT may be obscured.[5]

Table 1. Spectroscopic properties of **3**, **4** and **5** in MeCN at R.T.

Complex	Abs. [nm]/(ε x 10^4 [$M^{-1}cm^{-1}$])	Luminescence at R.T. λ_{exc} [nm]	λ_{em} [nm]	τ[a] [ns]	ν_{CO} [cm^{-1}] A′(1)	A′(2)	A″	TRIR ν_{CO} [cm^{-1}] Parent bands	Transient bands
3	454/(1.16)	450	635	240	–	–	–	–	–
4	335/(0.20)	450	623	n.d.[b]	2022	1915	1898	2010, 1905, 1890	2055, 1978, 1947
		335	375						
5	450/(1.56)	450	675	217	2022	1917	1899	2013, 1909, 1890	2010, 1875

[a] Non-degassed, [b] Emission too weak to determine.

2.2.3. Infrared Spectroscopy

A mononuclear rhenium tricarbonyl complex can exist as one of two structural isomers, *fac* or *mer*. Typically *fac* and *mer* isomers of tri-carbonyl complexes are characterised by IR spectroscopy and exhibit very different CO stretching frequency bands. The FTIR spectra of the mononuclear rhenium tricarbonyl complexes and ruthenium-rhenium hetero-dinuclear complexes discussed here show three bands in the region of 1850–2050 cm^{-1}.[26,27] Generally *fac*-isomers have three intense IR bands in the metal carbonyl region whereas *mer*-isomers show two intense IR υ(CO) stretching modes, in addition to a weaker mode.[28] The IR bands for the synthesised metal carbonyl complexes discussed here are shown in the Supporting Information, with the IR stretching vibrations for the metal carbonyl bands featured in Table 1. All IR spectra were recorded in acetonitrile.

2.2.4. Photophysical Studies

Room temperature emission spectra were recorded in spectrophotometric grade acetonitrile at 298 K and the results are summarised in Table 1. Following excitation of compound **4** at 450 nm, a very weak emission was observed at 623 nm, in agreement with studies on other (bpy)$Re(CO)_3Cl$ type complexes.[29,30] The emission spectra for compounds **3** and **5**, as displayed in Figure 2, were obtained following excitation at 450 nm. The maximum emission of complex **3** was observed at 635 nm, while the Ru–Re dinuclear system **5** demonstrated a red shift in emission to $\lambda_{max} = 675$ nm. The lifetimes of both complexes **3** (240 ns) and **5** (217 ns) are similar, following excitation at 360 nm. This observation indicates that the interaction between the Ru and the Re centre is limited.

2.2.5. Picosecond Time-Resolved Infrared (TRIR) Spectroscopy

A picosecond time resolved infrared (TRIR) study of compounds **4** and **5** was undertaken in acetonitrile at 20±2 °C. The TRIR spectra were obtained following excitation with λ = 320 (**4**) or 450 nm (**5**), with the resulting band positions included in table 1.

Excitation of compound **4** ($\lambda_{exc} = 320$ nm) results in depletion of the parent bands at 2010, 1905, 1890 cm^{-1} within 1 ps, together with the formation of new stretching vibrations at 2055, 1978 and 1947 cm^{-1} (Figure 3a). Within 20 ps, the latter broad bands sharpen, accompanied by a blue shift, indicating vibrational cooling.[31] There is no evidence for recovery of the parent bands on this time scale. The shifting of IR bands to higher energy than their ground state counterparts is commonly observed in polypyridine rhenium tricarbonyl complexes.[32–34] For example, in the case of (4,4′-bpy)$_2Re(CO)_3Cl$ or (bpy)$Re(CO)_3Cl$ (**2**), a shift in transient bands to higher wavenumbers was previously assigned to population of a charge transfer state.[27,31,35–37] Hence, the positive shifts of the ν_{CO} bands for **4** formed upon excitation agrees with previous studies on similar complexes, Consequently, these new bands are assigned to a triplet Re→qpy charge transfer excited state. The excited state is long-lived and persists for >1 ns (the limit of the time resolved apparatus). Similar compounds have long lived excited states that may persist for hundreds of nanoseconds.[38,39]

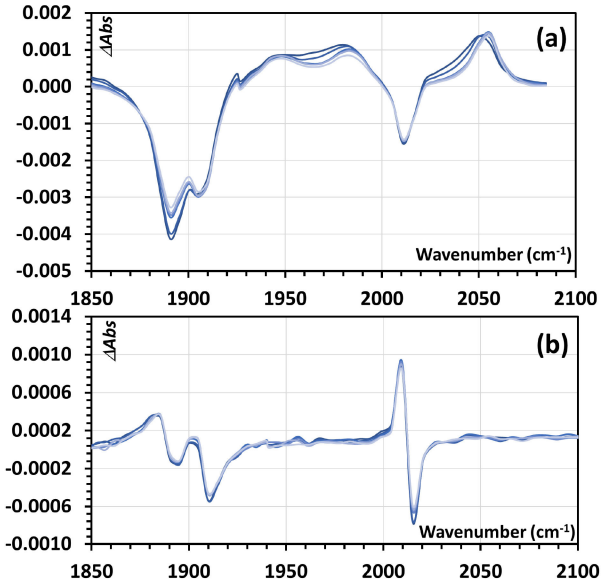

Figure 3. Time-resolved infrared difference spectra following laser photolysis for **4** ($\lambda_{exc} = 320$ nm, left) and **5** ($\lambda_{exc} = 450$ nm, right) in acetonitrile.(at 5, 10, 50, 90, 150 and 400 ps, respectively).

Excitation of the dinuclear compound **5** at $\lambda_{exc} = 450$ nm (shown in Figure 3b) results in depletion of the parent bands at 2013, 1909, 1890 cm^{-1} within the laser pulse. The new bands are observed at lower wavenumbers (2010 and 1875 cm^{-1}) when compared to the ground state, indicating an increase in electron density at the Re centre, resulting in an increase in π-back bonding to the CO ligands. Similar observations were noted by Ward and co-workers for their $[(bpy)_2Ru^{II}(AB)Re^{I}(CO)_3Cl]^{2+}$ and $[Cl(CO)_3Re^{I}(AB)Ru^{II}(bpy)_2]^{2+}$ complexes, where AB is an asymmetric 'bent' bridging ligand 2,2′:3′,2″:6″,2‴-quaterpyridine (which differs to the linear quaterpyridine bridging ligand in this study).[40] Irradiation into either the Re or Ru MLCT transition of $[(bpy)_2Ru^{II}(AB)Re^{I}(CO)_3Cl]^{2+}$ resulted in depletion of the parent bands at 1902, 1918 and 2023 cm^{-1} and formation of new signals at 1888, 1910 and 2016 cm^{-1}. The shift of the ν_{CO} bands to lower wavenumbers was assigned to the formation of the Ru→AB bridging ligand based MLCT state $[(bpy)_2Ru^{III}(AB)Re^{I}(CO)_3Cl]^{2+}$. However TRIR data for another isomer $[Cl(CO)_3Re^{I}(AB)Ru^{II}(bpy)_2]^{2+}$ showed bleaching of the parent bands at 1902, 1922 and 2028 cm^{-1} and the formation of new bands at 1892, 1912 and 2018 cm^{-1} as well a broad band at 1965 cm^{-1}. These observations have been assigned to the formation of both Re and Ru based MLCT excited states $[Cl(CO)_3Re^{II}(AB)^{-}Ru^{II}(bpy)_2]^{2+}$ and $[Cl(CO)_3Re^{I}(AB)^{-}Ru^{III}(bpy)_2]^{2+}$.

Hence, it can be concluded from the TRIR spectra of compound **5,** that the shift to lower frequency of all the ν_{CO} bands formed upon excitation at 450 nm agrees with the previous studies on similar $[(bpy)_2Ru^{II}(AB)Re^{I}(CO)_3Cl]^{2+}$ type complexes. Consequently these new bands are assigned to a

Ru^{II} to qpy bridging ligand based MLCT state $[(bpy)_2Ru^{III}(qpy)Re^{I}(CO)_3Cl]^{2+}$.

2.3. Computational Studies

The electronic structures of the fifty lowest singlet electronic excited states were calculated using TD-DFT methods at the optimised singlet geometry.[41–43] The vertical excitation energies and oscillator strengths obtained from these calculations were then used to simulate the UV/visible spectrum of **5.** This was done by placing Gaussian functions at each vertical excitation energy with a height of corresponding to the calculated oscillator strength and a width at half height of 3000 cm^{-1}. The resulting spectrum is presented in Figure 4 along with the

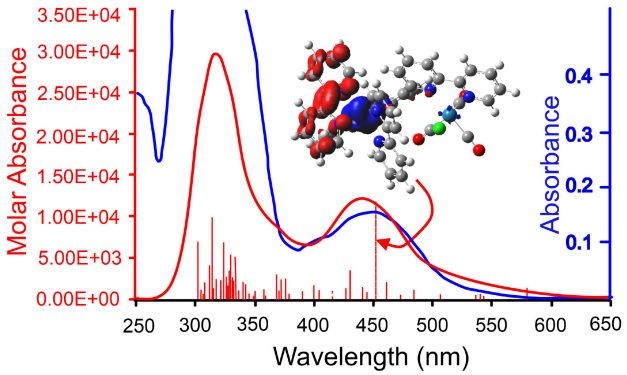

Figure 4. The experimental UV/Vis spectrum of **5** (1×10^{-5} M) in acetonitrile (blue; vertical scale in absorbance also blue) and the simulated spectrum (red; vertical scale molar absorbance also red) along with the vertical transition energies (red vertical lines) to the fifty lowest energy singlet excited states. The electron density difference map for the fifteenth singlet excited state is also presented in which the region of reduced electron density relative to the ground state is indicated in blue and the region of increased electron density is indicted in red.

experimental spectrum obtained in acetonitrile solution. The vertical excitation energies are also highlighted as vertical red lines and the electron density difference map of the 15th singlet excited state (S_{15}) is also included. This can be classified as a Ru to bpy charge-transfer state and corresponds to the most intense transition at 451 nm close to the low energy $\lambda_{max.}$ in both the simulated and experimental spectrum. It is clear that the B3LYP/LanL2DZ/TD-DFT method accurately models the experimental UV/visible spectrum.

The structure of the lowest energy triplet state of complex **5** was optimized. TD-DFT methods were again employed to calculate the transition energies to the lowest triplet electronic excited states. In addition, the lowest energy singlet species at this triplet geometry was also optimised. Using these data it is possible to calculate the number of triplet excited states at or below the energy of the S_{15} state. These excited states (T_0 to T_3), are presented in the energy level diagram in Figure 5. It is generally accepted that following population of a ruthenium to bpy charge-transfer singlet excited state the system rapidly undergoes intersystem crossing (ISC) to the triplet surface.[44] In

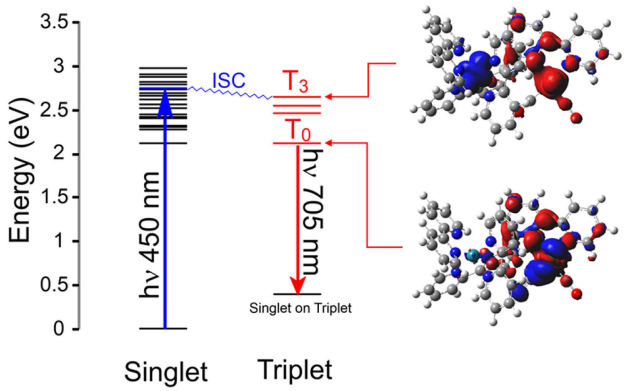

Figure 5. The singlet energy levels (black) obtained from TD-DFT methods for compound **5** using the optimized ground-state geometry (B3LYP/LanL2DZ) showing excitation (450 nm) into S_{15} followed by intersystem crossing to the triplet surface (red levels) with the singlet energy at the triplet geometry indicated (black) below the triplet levels; electron density difference maps are presented for T_0 and T_3 where the electron density of the lowest energy singlet state at the triplet geometry was subtracted from the appropriate triplet state electron density, regions of reduced electron density are indicated in blue and those of increased electron density are indicted in red.

energy terms the closest triplet state to the S_{15} is the T_3 state, which is predominantly ruthenium to rhenium charge transfer in character while the lowest energy triplet state (T_0) has rhenium to ligand charge-transfer character.

The infrared spectrum of the lowest energy triplet state was then simulated. To compare with the experimental TRIR data, the calculated spectrum of the singlet ground state was then subtracted from the simulated triplet state spectrum. (Figure 6).

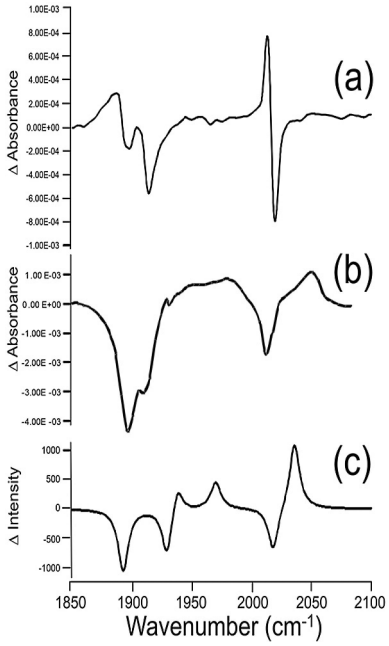

Figure 6. A comparison of the TRIR spectrum obtained following excitation of a) **5** at 450 nm, b) **4** at 320 nm (both obtained in acetonitrile) and c) the calculated difference spectrum for the T_0 excited state of **5**.

It is clear that in the calculated difference spectrum for the T_0 state of **5** the ν_{CO} bands behave in a manner similar to that of **4** when irradiated using 320 nm light, particularly in respect of the shift to higher energy of the highest energy ν_{CO} band. In contrast, the ν_{CO} bands shift to lower energy following 450 nm excitation of complex **5**. These results suggest that upon excitation of **5** at 450 nm the state that is ultimately populated is not the lowest energy triplet state but rather a higher energy triplet state.

Finally the behaviour of the optically accessible singlet excited states was modelled along the *trans*-CO-loss reaction coordinate. A relaxed potential energy scan was then performed where the trans-CO ligand to metal distance was increased in 0.1 Å increments. At each point along this reaction coordinate a TD-DFT calculation was performed to estimate the energies of the twenty lowest energy singlet excited states (vertical excitation energies in the range 2 to 3 eV corresponding to the photon energies used in the photochemical experiments). The results of these calculations are presented in Figure S12 and confirm that no singlet excited state in this energy range presents an accelerating energy profile to loss of the *trans*-CO ligand. Consequently, the calculations suggest that photochemical excitation of this complex will not result in *trans*-CO loss.

2.4. Cyclic Voltammetry

The location of the reduction potentials of complexes **4** and **5** is of prime importance for the efficiency of the quenching process in the photocatalytic CO_2 reduction cycle. The cyclic voltammetry of these compounds is shown in Figure 7 and Table 2.

The most positive cathodic feature of **4** is a quasireversible first reduction at −1.62 V vs Fc/Fc^+. This wave is generally assigned to a ligand based reduction, as observed in the case of **2**.[45–47] At more negative potentials (See Figure S13), further quasi- or irreversible reductions are observed. This contrasts with a more pronounced irreversible reduction of **2**.[48] Ruthenium trisbipyridine complexes typically exhibit three reversible ligand based reductions.[25,49–52] In the case of **5**, the first two quasireversible reductions are observed at −1.4 V and −1.62 V vs Fc/Fc^+. Unresolved and irreversible reductions observed more negative than −1.62 V vs Fc/Fc* are not further considered.

A key observation is that the reduction of compound **4** appears at a similar potential as the second reduction of **5** as shown in Figure 7a. This suggests that the second reduction of **5** may be assigned to the Re-qpy moiety of the complex. This indicates that there is limited communication between the Ru and Re subunits.[5,10,53] For **5** the first (and qpy-based) reduction at approximately −1.4 V vs Fc/Fc^+ is very similar to that observed for the dinuclear $[(bpy)_2Ru(qpy)Ru(bpy)_2]^{4+}$ compound.[54] The qpy-based reductions of **5** are shifted anodically by 340 mV and 120 mV relative to **1** and **2** respectively. This is related to the presence of the qpy ligand that has stronger electron withdrawing properties than the bpy analogue.[55,56]

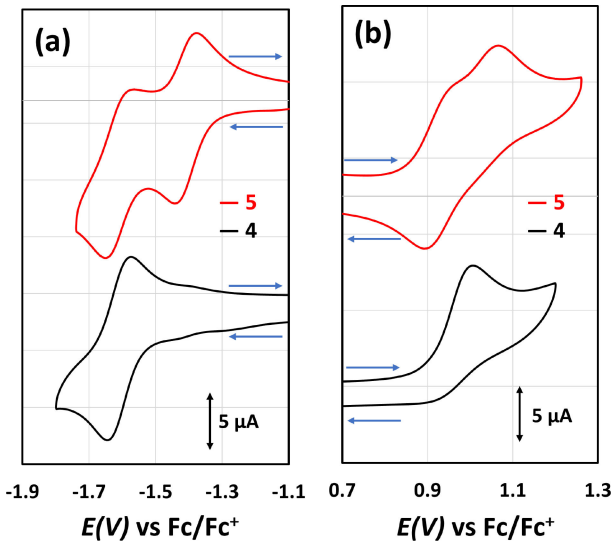

Figure 7. a) Reductive and b) oxidative cyclic voltammetry of **5** and **4** (0.75 mM) in MeCN with 0.1 M $TBAPF_6$ (as supporting electrolyte). a) Cyclic voltammograms were recorded using glassy carbon (3 mm diameter) as the working electrode, Pt as the counter electrode and an Ag/Ag^+ reference electrode at scan rate $\nu = 100\ mV\,s^{-1}$. All potential values were further calibrated against Fc/Fc^+.

Table 2. Summary of the first oxidation and reduction potentials vs Fc/Fc^+ of the assessed complexes at scan rate = 100 mV s^{-1} in MeCN/0.1 M $TBAPF_6$.[a]

Complex	Ru $(L/L^-)_1$ [V]	Re (L/L^-) [V]	$Ru^{II/III}$ [V]	$Re^{I/II}$ [V]
5	−1.4(q)	−1.62(q)	0.93	1.07(i)
4	–	−1.62(q)	–	1.01(i)
2	–	−1.74	–	0.98(i)
1	−1.74	–	0.89	–

[a] i = irreversible oxidation at $\nu = 100\ mV\,s^{-1}$, E_{pa} displayed. q = quasireversible process, $E_{1/2}$ displayed. All other values are $E_{1/2}$ values.

The oxidative voltammetry of compounds **4** and **5** is shown in Figure 7b. Compound **4**, as observed for **2**, undergoes an irreversible $Re^{I/II}$ metal-based oxidation at 1.01 V vs Fc/Fc^+.[57] Regarding **5**, a quasireversible oxidation and an irreversible oxidation are observed. For comparison, $[(bpy)_2Ru(qpy)Ru(bpy)_2]^{4+}$ demonstrates a quasireversible oxidation with $E_{1/2}$ of approximately 0.95 V vs Fc/Fc^+,[54] associated with the $Ru^{II/III}$ redox couple. For other Ru–Re complexes the first oxidation has been reported to occur at the Ru centre.[10,58] Additionally, the first oxidations of **1** and **2** occur with E_{pa} of 0.94 V and 0.98 V vs Fc/Fc^+ respectively. Further to this, as shown in Figure S14, there appears to be some reversibility of the second oxidation at higher scan rates.

2.5. Photocatalytic CO_2 Reduction

The photocatalytic properties of mixtures containing **1** and **2** were investigated and compared to those of the dinuclear complex **5**. Initial solvent and sacrificial electron donor studies were undertaken to optimise the conditions for photocatalysis using the intermolecular system of complexes **1** and **2** and the

results obtained appear in Figure S16. In agreement with the literature,[17,59] TEOA as a sacrificial electron donor (1:5 v/v) provides higher TON_{CO} values compared to TEA (TON_{CO} <1 in either DMF or MeCN). DMF as solvent yielded a TON_{CO} of 35 while with DMA a value of 14 was obtained, while MeCN gave TON_{CO} values of up to 10. 1-benzyl-1,4-dihydronicotinamide (BNAH) has previously been shown to enhance CO production.[60] However, when the irradiation source was 355 nm, the mixture of **1** and **2** in DMF/TEOA (5:1) with 0.1 M BNAH produced <1 TON_{CO}, which contrasts with a TON_{CO} = 9 when the irradiation sources was changed to 470 nm. This may be due to an inner filter effect, as BNAH absorbs strongly at 355 nm.[61]

The photocatalytic efficiency of the intramolecular assembly **5** was assessed in DMF/TEOA (5:1), (as shown in Figure 8). Over

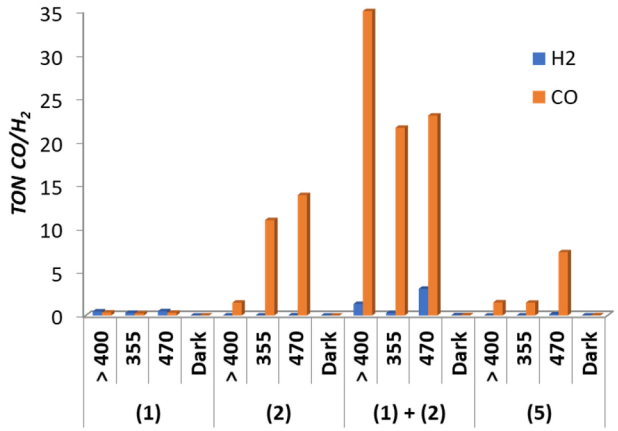

Figure 8. Photocatalytic CO_2 reduction performed with 100 μM **5**, 134 μM **1** + 100 μM **2**, 134 μM **1**, and 100 μM **2** in DMF/TEOA (5:1 v/v); irradiation time of 21 hours.

the 21 hour irradiation period, TON_{CO} values of 7 (λ = 470 nm) were obtained, but drops to <2 for 355 nm or >400 nm irradiation. In this intramolecular assembly, the activity towards CO_2 reduction was very limited when compared with the results obtained for the intermolecular mixture of **1** and **2**. The intermolecular approach generated higher TON_{CO} values of 23 and 22 at λ = 470 nm and λ = 355 nm respectively. A further study was undertaken in MeCN/TEA (5:1). As with the intermolecular systems containing complexes **1** and **2**, the intramolecular mixture containing complex **5** failed to produce any significant amount of CO (as shown in Figure S17).

Reductive quenching of the photosensitiser's excited state has been commonly reported as a reason for efficient photocatalytic CO_2 reduction.[2,3,62] Following reductive quenching of the excited state photosensitiser by the sacrificial electron donor, the reduced photosensitiser in turn reduces the catalyst, whereby the reduction of the photosensitiser is close to or more negative than that of the catalyst.[59] With respect to intramolecular photocatalytic Ru–Re CO_2 reduction catalysts, it has been shown in the literature that a conjugated bridging system between the Ru and Re units yields an anodic shift in the first reductions of the photosensitiser and catalyst, which is concurrent with lower photocatalytic activity of the complexes.[5,63,64] A vinyl-bridged Ru_2-Re trinuclear complex, reported by Ishitani and co-workers, produced similar TON_{CO} to its saturated homologue. However, the vinyl units undergo saturation during the photocatalysis experiments.[65]

2.6. Energetic Feasibility of Oxidative and Reductive Quenching

2.6.1. Oxidative Quenching

Excitation of the complex was undertaken at 470 nm, thereby selectively irradiating the Ru–L ^{1}MLCT. The resulting emission and absorbance spectra, as acquired in MeCN, are shown in Figure S15. An approximate $E_{0\text{-}0}$ value of 569 nm was obtained,[66,67] equating to 2.18 eV. The first oxidation of **5** occurs with $E_{1/2}$ of 0.93 V vs Fc/Fc^+. Therefore, as per Equation (1),[68,69] the [**5**]*/[**5**(Ru^+Re^-)] excited state oxidation potential occurs at −1.25 V vs Fc/Fc^+. The first two ground state reduction potentials of **5** are −1.4 V and −1.62 V vs Fc/Fc^+ (Table 2). These processes, with comparison to **4**, are Ru–L based and Re–L based reductions respectively. Therefore, intramolecular oxidative quenching of Ru by Re subunits is not expected to proceed.[70,71]

$$E(PS^*/PS^+) = E(PS/PS^+) - E_{0\text{-}0} \quad (1)$$

2.6.2. Reductive Quenching

Quenching experiments of **5** with TEOA were not undertaken. However, the first (and Ru–L based) reduction of **5** occurs at −1.4 V vs Fc/Fc^+ and the $E_{0\text{-}0}$ was approximated as 2.18 eV. The excited state reduction potential of **5** (as calculated by Equation (2)[51,72]),(i.e. [**5**]*/[**5**]$^-$) is +0.78 V vs Fc/Fc^+. As the oxidation potential of TEOA is +0.33 V,[68] this reaction is expected to proceed.[2]

$$E(PS^*/PS^-) = E(PS/PS^-) + E_{0\text{-}0} \quad (2)$$

However, as electrochemical results for **4** imply that the second reduction within **5** is a Re ligand based reduction, which occurs at 0.22 V more negative to that of the Ru–L based reduction (−1.62 V and −1.4 V vs Fc/Fc^+ respectively). Therefore, though quenching of the excited state of **5** by TEOA is suggested to proceed, the subsequent reduction of the Re moiety by the Ru moiety is not. The intermolecular approach with **1** and **2** was assessed in the same manner, and is suggested to proceed by reductive quenching (**1** $E_{0\text{-}0}$ of 2.26 eV).

3. Conclusions

In this contribution, the photocatalytic potential of the intramolecular RuRe (**5**) assembly towards CO_2 reduction was

investigated and compared to the intermolecular system of **1** and **2**. Generally within Ru–Re complexes, weak interactions between the photosensitiser and the catalytic centre often leads to an effective photocatalytic system for CO_2 reduction. Although the electronic coupling between the Ru and the Re moiety in compound **5** is weak (as indicated by emission studies, TRIR, electrochemistry and quantum chemical calculations), the results obtained in these studies show that the highest TON values are obtained with the intermolecular approach. The most likely reason for the low activity of compound **5** is obtained from the electrochemical studies, which indicates that neither oxidative or reductive quenching is likely, whereas reductive quenching is a favoured process in the intermolecular approach.

Experimental Section

^{1}H NMR (400 MHz) spectra were recorded in deuterated solvents (d_6-DMSO, d_3-MeCN) on a Bruker AC400 NMR Spectrometer with TMS or residual solvent peaks as reference. The XWIN-NMR processor and ACDLABS 12.0 NMR processor software were employed to process the free induction decay (FID) profiles. The H–H 2D COSY NMR involved the accumulation of 128 FIDs of 16 scans. Elemental analysis (CHN) was carried out using Exador Analytical CE440 by the Microanalytical Department, University College Dublin, Ireland. UV-Vis absorption spectra were recorded on a Shimadzu 3100 UV-Vis/NIR spectrophotometer interfaced to an Elonex PC575 desktop computer using 1 cm path length quartz cell. The detection wavelength was 190–800 nm. The ASCII data for each UV-Vis spectra were further processed using Excel 2016 software. Emission spectra were recorded on a Perkin-Elmer LS50B luminescence spectrophotometer. The solvent used for the room temperature emission spectroscopy was spectroscopic grade MeCN. All spectra were initially generated by Perkin-Elmer FL Winlab custom built software and further the ASCII data were processed by Excel 2016 software. The optical densities of all sample solutions were approximately 0.15 A.U.

The ps-TRIR apparatus was previously reported by us, but a general overview is as follows.[73] UV pump and mid-IR probe pulses were generated by a Ti:sapphire laser (repetition rate 1 kHz). The UV pump pulse at 400 or 320 nm excitation typically had pulse energies in the range 0.8 to 1 μJ, and was generated by second harmonic generation (SHG). IR probe pulses were generated by difference frequency generation (DFG) of the signal and idler from a BBO-based OPA in $AgGaS_2$. The delay positions were scanned by mechanically adjusting the beam-path of the UV pump using a translation stage. The temporal resolution of 200 fs has been obtained from the FWHM of the pump–probe cross-correlation function recorded in a 1 mm thick layer of Si placed in a sample cell identical to that used for the solutions.

All electrochemical analyses were undertaken with CH instruments 600e and 750c potentiostats. Unless otherwise stated, all voltammograms were undertaken at 100 mV s^{-1} scan rate. Voltammetry was undertaken in a custom-built V-shaped cell using of a 3-electrode setup with a 3 mm diameter glassy carbon working electrode, coiled platinum wire counter electrode and Ag/Ag^+ non-aqueous reference electrode (uncoated Ag wire with 0.01 M $AgNO_3$, 0.1 M $TBAPF_6$ in MeCN filling solution) and undertaken in Ar-purged anhydrous MeCN with 0.1 M $TBAPF_6$ as supporting electrolyte. All potentials were referenced with respect to the $Fe^{2+/3+}$ couple of ferrocene. The synthesis of **3**, the precursor to **5** has been reported previously.[19]

Synthesis

Synthesis of [(qpy)Re(CO)$_3$Cl] (4)

102 mg (0.33 mmol) of qpy and 50 mL anhydrous toluene were added to a 100 mL round-bottom flask under N_2 atmosphere. 100 mg (0.77 mmol) of $Re(CO)_5Cl$ was added slowly over a period of 1 hour to the solution with slow stirring of the reaction mixture. After the addition of $Re(CO)_5Cl$, the reaction mixture was brought to reflux temperature for 2 hours under a N_2 atmosphere. The reaction was stopped and cooled to room temperature after 2 hours. An orange colour precipitate formed and was washed with cold toluene to remove the unreacted $[Re(CO)_5Cl]$. The product was then recrystallised from an MeCN/diethyl-ether solvent mixture to remove the dinuclear $(qpy)[Re(CO)_3Cl]_2$ species formed as a by-product during the reaction. The infra-red (IR) spectra of the product was checked and recorded using MeCN to confirm the formation of product. **Yield:** 152 mg, 0.25 mmol, 75%. ^{1}H NMR (400 MHz, DMSO-d_6) δ ppm 7.53 (ddd, J = 7.39, 4.74, 1.26 Hz, 1 H) 7.76–7.83 (m, 1 H) 8.03 (td, J = 7.71, 1.77 Hz, 1 H) 8.34–8.41 (m, 1 H) 8.50 (d, J = 8.08 Hz, 1 H) 8.53–8.62 (m, 2 H) 8.76 (dd, J = 3.66, 0.88 Hz, 1 H) 8.82 (dd, J = 8.59, 2.02 Hz, 1 H) 8.87 (d, J = 8.34 Hz, 1 H) 8.91–8.95 (m, 2 H) 9.05–9.10 (m, 1 H) 9.26 (dd, J = 2.27, 0.76 Hz, 1 H) 9.32 (d, J = 2.27 Hz, 1 H) IR ν_{co} CH_3CN: 2022, 1915, 1898 cm^{-1}.Elemental analysis for $C_{23}H_{14}ClN_4O_3Re$. M.W. = 616.04; Calc: C 44.84, H 2.29, N 9.09. Found: C 45.05, H 2.20 and N 9.41%.

Synthesis of [(bpy)$_2$Ru(μ-qpy)Re(CO)$_3$Cl](PF$_6$)$_2$ (5)

40 mL of spectroscopic grade ethanol was purged with nitrogen for 30 minutes. 77 mg (0.075 mmol) of $[(bpy)_2Ru(qpy)](PF_6)_2$ (**1**) and 32.8 mg (0.09 mmol) of $[Re(CO)_5Cl]$ were added to the purged ethanol. The reaction mixture was then refluxed in the dark for a further 6 hours under a nitrogen atmosphere. The reaction was monitored by TLC and IR. The solvent was removed by rotary evaporation after 6 hours of reaction. The crude product was washed with *n*-pentane and diethyl ether. The bright red coloured product was further purified by recrystallisation from an acetone/toluene solution. **Yield:** 86 mg, 0.065 mmol, 87%. ^{1}H NMR (400 MHz, DMSO-d_6) δ ppm 1.32–1.39 (m, 12 H), 4.41 - 4.48 (m, 8 H), 7.51–7.61 (m, 1 H), 7.75–8.05 (m, 10 H), 8.07–8.20 (m, 1 H), 8.23–8.31 (m, 1 H), 8.36 (t, J = 8.34 Hz, 1 H), 8.62–8.70 (m, 1 H), 8.73–8.90 (m, 4 H), 8.98–9.05 (m, 2 H), 9.08 (dd, J = 8.59, 3.03 Hz, 1 H), 9.19 (d, J = 16.93 Hz, 1 H), 9.25 (d, J = 8.08 Hz, 1 H), 9.32 (d, J = 8.34 Hz, 2 H). IR ν_{co} in CH_3CN: 2022, 1917, 1899 cm^{-1}. Elemental analysis for $C_{43}H_{30}ClF_{12}N_8O_3P_2F_{12}RuRe$. 4 H_2O Mw 1391.48. Calc. 37.12, H 2.75, N 8.05; Found C 37.48, H 2.44, N 7.45%.

Computational Studies

All calculations were performed using either Gaussian 09[74] or Gaussian 16[75] programme suites. The hydrid density functional B3LYP[76–78] was used for all calculations coupled with the LanL2DZ basis set.[79–82] The initial molecular structure was obtained from molecular modelling techniques and was then optimized to tight convergence criteria at the B3LYP/LanL2DZ model chemistry. The UV/visible spectra were simulated using the results of TD-DFT calculations by convolution of Gaussian functions (3000 cm^{-1} band width at half-height) with the calculated stick spectra.[83,84] Relaxed potential energy scans incrementally increased the Re to *trans*-CO distance from the optimized value in ten steps of 0.1 Å allowing all other structural parameters to optimize. This provided a set of ten molecular coordinates which were then used in TD-DFT calculations of the excitation energies of the twenty low energy singlet excited states. The energy of the excited states were corrected for changes

in the ground state energy along this reaction coordinate providing potential energy profiles for each excited state as the *trans*-CO bond lengthened.

Acknowledgements

The authors wish to acknowledge the SFI/HEA Irish Centre for High-End Computing (ICHEC) for the provision of computational facilities and support. The authors thank the Amsterdam Laboratory under EU access-LLAMS-1961. We would like also thank the Environmental Protection Agency (EPA Grant 2008-ET-MS-3-S2) and SFI/TIDA/E2763, SFI/TIDA/2435 for financial support.

Conflict of Interest

The authors declare no conflict of interest.

Keywords: carbon dioxide reduction · photocatalysis · picosecond time-resolved infrared spectroscopy · quantum chemical calculations

[1] K. W. Thoning, P. P. Tans, W. D. Komhyr, *J. Geophys. Res. [Atmos.]* **1989**, *94*, 8549–8565.
[2] Y. Yamazaki, H. Takeda, O. Ishitani, *J. Photochem. Photobiol. C Photochem. Rev.* **2015**, *25*, 106–137.
[3] Y. Tamaki, O. Ishitani, *ACS Catal.* **2017**, *7*, 3394–3409.
[4] G. Sahara, O. Ishitani, *Inorg. Chem.* **2015**, *54*, 5096–5104.
[5] B. Gholamkhass, H. Mametsuka, K. Koike, T. Tanabe, M. Furue, O. Ishitani, *Inorg. Chem.* **2005**, *44*, 2326–2336.
[6] Y. Tamaki, K. Koike, T. Morimoto, O. Ishitani, *J. Catal.* **2013**, *304*, 22–28.
[7] K. Koike, S. Naito, S. Sato, Y. Tamaki, O. Ishitani, *J. Photochem. Photobiol. Chem.* **2009**, *207*, 109–114.
[8] S. Sato, K. Koike, H. Inoue, O. Ishitani, *Photochem. Photobiol. Sci.* **2007**, *6*, 454–461.
[9] Y. Tamaki, K. Watanabe, K. Koike, H. Inoue, T. Morimoto, O. Ishitani, *Faraday Discuss.* **2012**, *155*, 115–127.
[10] E. Kato, H. Takeda, K. Koike, K. Ohkubo, O. Ishitani, *Chem. Sci.* **2015**, *6*, 3003–3012.
[11] A. Nakada, K. Koike, T. Nakashima, T. Morimoto, O. Ishitani, *Inorg. Chem.* **2015**, *54*, 1800–1807.
[12] Y. Tamaki, K. Koike, O. Ishitani, *Chem. Sci.* **2015**, *6*, 7213–7221.
[13] C. D. Windle, M. W. George, R. N. Perutz, P. A. Summers, X. Z. Sun, A. C. Whitwood, *Chem. Sci.* **2015**, *6*, 6847–6864.
[14] N. Elgrishi, M. B. Chambers, X. Wang, M. Fontecave, *Chem. Soc. Rev.* **2017**, *46*, 761–796.
[15] A. Paul, D. Connolly, M. Schulz, M. T. Pryce, J. G. Vos, *Inorg. Chem.* **2012**, *51*, 1977–1979.
[16] Y. Kuramochi, M. Kamiya, H. Ishida, *Inorg. Chem.* **2014**, *53*, 3326–3332.
[17] T. Morimoto, T. Nakajima, S. Sawa, R. Nakanishi, D. Imori, O. Ishitani, *J. Am. Chem. Soc.* **2013**, *135*, 16825–16828.
[18] A. Gorczyński, J. M. Harrowfield, V. Patroniak, A. R. Stefankiewicz, *Chem. Rev.* **2016**, *116*, 14620–14674.
[19] N. Das, G. S. Bindra, A. Paul, J. G. Vos, M. Schulz, M. T. Pryce, *Chem. Eur. J.* **2017**, *23*, 5330–5337.
[20] D. A. Bardwell, F. Barigelletti, R. L. Cleary, L. Flamigni, M. Guardigli, J. C. Jeffery, M. D. Ward, *Inorg. Chem.* **1995**, *34*, 2438–2446.
[21] R. A. Kirgan, B. P. Sullivan, D. P. Rillema, in *Photochem. Photophysics Coord. Compd. II* (Eds.: V. Balzani, S. Campagna), Springer Berlin Heidelberg, **2007**, pp. 45–100.
[22] S. Záliš, C. Consani, A. E. Nahhas, A. Cannizzo, M. Chergui, F. Hartl, A. Vlček, *Inorganica Chim. Acta* **2011**, *374*, 578–585.
[23] R. L. Cleary, K. J. Byrom, D. A. Bardwell, J. C. Jeffery, M. D. Ward, G. Calogero, N. Armaroli, L. Flamigni, F. Barigelletti, *Inorg. Chem.* **1997**, *36*, 2601–2609.
[24] D. P. Rillema, G. Allen, T. J. Meyer, D. Conrad, *Inorg. Chem.* **1983**, *22*, 1617–1622.
[25] K. Kalyanasundaram, *Coord. Chem. Rev.* **1982**, *46*, 159–244.
[26] L. W. Houk, G. R. Dobson, *Inorg. Chem.* **1966**, *5*, 2119–2123.
[27] D. R. Gamelin, M. W. George, P. Glyn, F.-W. Grevels, F. P. A. Johnson, W. Klotzbuecher, S. L. Morrison, G. Russell, K. Schaffner, J. J. Turner, *Inorg. Chem.* **1994**, *33*, 3246–3250.
[28] S. Sato, T. Morimoto, O. Ishitani, *Inorg. Chem.* **2007**, *46*, 9051–9053.
[29] A. El Nahhas, C. Consani, A. M. Blanco-Rodríguez, K. M. Lancaster, O. Braem, A. Cannizzo, M. Towrie, I. P. Clark, S. Záliš, M. Chergui, et al., *Inorg. Chem.* **2011**, *50*, 2932–2943.
[30] D.-I. Won, J.-S. Lee, J.-M. Ji, W.-J. Jung, H.-J. Son, C. Pac, S. O. Kang, *J. Am. Chem. Soc.* **2015**, *137*, 13679–13690.
[31] D. M. Dattelbaum, K. M. Omberg, J. R. Schoonover, R. L. Martin, T. J. Meyer, *Inorg. Chem.* **2002**, *41*, 6071–6079.
[32] A. Gabrielsson, F. Hartl, H. Zhang, J. R. Lindsay Smith, M. Towrie, Vlček Antonín, R. N. Perutz, *J. Am. Chem. Soc.* **2006**, *128*, 4253–4266.
[33] G. Li, K. Parimal, S. Vyas, C. M. Hadad, A. H. Flood, K. D. Glusac, *J. Am. Chem. Soc.* **2009**, *131*, 11656–11657.
[34] J. R. Schoonover, C. A. Bignozzi, T. J. Meyer, *Coord. Chem. Rev.* **1997**, *165*, 239–266.
[35] D. J. Liard, M. Busby, P. Matousek, M. Towrie, A. Vlček, *J. Phys. Chem. A* **2004**, *108*, 2363–2369.
[36] A. Vlček Jr, I. R. Farrell, D. J. Liard, P. Matousek, M. Towrie, A. W. Parker, D. C. Grills, M. W. George, *J. Chem. Soc. Dalton Trans.* **2002**, 701–712.
[37] M. W. George, F. P. A. Johnson, J. R. Westwell, P. M. Hodges, J. J. Turner, *J. Chem. Soc. Dalton Trans.* **1993**, 2977–2979.
[38] L. A. Worl, R. Duesing, P. Chen, L. D. Ciana, T. J. Meyer, *J. Chem. Soc. Dalton Trans.* **1991**, *0*, 849–858.
[39] K. S. Schanze, D. Brent MacQueen, T. A. Perkins, L. A. Cabana, *Coord. Chem. Rev.* **1993**, *122*, 63–89.
[40] J. R. Schoonover, A. P. Shreve, R. B. Dyer, R. L. Cleary, M. D. Ward, C. A. Bignozzi, *Inorg. Chem.* **1998**, *37*, 2598–2601.
[41] R. E. Stratmann, G. E. Scuseria, M. J. Frisch, *J. Chem. Phys.* **1998**, *109*, 8218–8224.
[42] R. Bauernschmitt, R. Ahlrichs, *Chem. Phys. Lett.* **1996**, *256*, 454–464.
[43] M. E. Casida, C. Jamorski, K. C. Casida, D. R. Salahub, *J. Chem. Phys.* **1998**, *108*, 4439–4449.
[44] J. K. McCusker, *Acc. Chem. Res.* **2003**, *36*, 876–887.
[45] J. Hawecker, J.-M. Lehn, R. Ziessel, *J. Chem. Soc. Chem. Commun.* **1984**, 328–330.
[46] F. P. A. Johnson, M. W. George, F. Hartl, J. J. Turner, *Organometallics* **1996**, *15*, 3374–3387.
[47] A. I. Breikss, H. D. Abruña, *J. Electroanal. Chem. Interfacial Electrochem.* **1986**, *201*, 347–358.
[48] J. M. Smieja, C. P. Kubiak, *Inorg. Chem.* **2010**, *49*, 9283–9289.
[49] M. Zhou, J. Roovers, *Macromolecules* **2001**, *34*, 244–252.
[50] M. Zhou, G. P. Robertson, J. Roovers, *Inorg. Chem.* **2005**, *44*, 8317–8325.
[51] A. Juris, V. Balzani, F. Barigelletti, S. Campagna, P. Belser, A. von Zelewsky, *Coord. Chem. Rev.* **1988**, *84*, 85–277.
[52] T. Saji, S. Aoyagui, *J. Electroanal. Chem. Interfacial Electrochem.* **1975**, *58*, 401–410.
[53] L. Moreira, J. Calbo, J. Aragó, B. M. Illescas, I. Nierengarten, B. Delavaux-Nicot, E. Ortí, N. Martín, J.-F. Nierengarten, *J. Am. Chem. Soc.* **2016**, *138*, 15359–15367.
[54] Y. Halpin, L. Cleary, L. Cassidy, S. Horne, D. Dini, W. R. Browne, J. G. Vos, *Dalton Trans.* **2009**, 4146.
[55] E. Rousset, D. Chartrand, I. Ciofini, V. Marvaud, G. S. Hanan, *Chem. Commun.* **2015**, *51*, 9261–9264.
[56] C. Hansch, A. Leo, R. W. Taft, *Chem. Rev.* **1991**, *91*, 165–195.
[57] J. P. Bullock, E. Carter, R. Johnson, A. T. Kennedy, S. E. Key, B. J. Kraft, D. Saxon, P. Underwood, *Inorg. Chem.* **2008**, *47*, 7880–7887.
[58] G. Sahara, H. Kumagai, K. Maeda, N. Kaeffer, V. Artero, M. Higashi, R. Abe, O. Ishitani, *J. Am. Chem. Soc.* **2016**, *138*, 14152–14158.
[59] J.-M. Lehn, R. Ziessel, *Proc. Natl. Acad. Sci. USA* **1982**, *79*, 701–704.
[60] H. Ishida, K. Tanaka, T. Tanaka, *Chem. Lett.* **1988**, *17*, 339–342.
[61] Y. Tamaki, T. Morimoto, K. Koike, O. Ishitani, *Proc. Natl. Acad. Sci. USA* **2012**, *109*, 15673–15678.
[62] R. Reithmeier, C. Bruckmeier, B. Rieger, *Catalysts* **2012**, *2*, 544–571.
[63] Z.-Y. Bian, S.-M. Chi, L. Li, W. Fu, *Dalton Trans.* **2010**, *39*, 7884–7887.
[64] Z.-Y. Bian, H. Wang, W.-F. Fu, L. Li, A.-Z. Ding, *Polyhedron* **2012**, *32*, 78–85.
[65] Y. Yamazaki, A. Umemoto, O. Ishitani, *Inorg. Chem.* **2016**, *55*, 11110–11124.

[66] A. Islam, H. Sugihara, H. Arakawa, *J. Photochem. Photobiol. Chem.* **2003**, *158*, 131–138.
[67] W.-K. Huang, C.-W. Cheng, S.-M. Chang, Y.-P. Lee, E. Wei-Guang Diau, *Chem. Commun.* **2010**, *46*, 8992–8994.
[68] S. Jasimuddin, T. Yamada, K. Fukuju, J. Otsuki, K. Sakai, *Chem. Commun.* **2010**, *46*, 8466–8468.
[69] V. Balzani, G. Bergamini, S. Campagna, F. Puntoriero, in *Photochem. Photophysics Coord. Compd. I* (Eds.: V. Balzani, S. Campagna), Springer Berlin Heidelberg, **2007**, pp. 1–36.
[70] J. Schneider, K. Q. Vuong, J. A. Calladine, X.-Z. Sun, A. C. Whitwood, M. W. George, R. N. Perutz, *Inorg. Chem.* **2011**, *50*, 11877–11889.
[71] C. D. Windle, M. V. Câmpian, A.-K. Duhme-Klair, E. A. Gibson, R. N. Perutz, J. Schneider, *Chem. Commun.* **2012**, *48*, 8189.
[72] P. Ceroni, V. Balzani, in *Explor. Supramol. Syst. Nanostructures Photochem. Tech.* (Ed.: P. Ceroni), Springer Netherlands, **2012**, pp. 21–38.
[73] S. McMahon, S. Amirjalayer, W. J. Buma, Y. Halpin, C. Long, A. D. Rooney, S. Woutersen, M. T. Pryce, *Dalton Trans.* **2015**, *44*, 15424–15434.
[74] J. Frisch, G. W. Trucks, H. B. Schlegel, G. E. Scuseria, M. A. Robb, J. R. Cheeseman, G. Scalmani, V. Barone, B. Mennucci, G. A. Petersson, H. Nakatsuji, M. Caricato, X. Li, H. P. Hratchian, A. F. Izmaylov, J. Bloino, G. Zheng, J. L. Sonnenberg, M. Hada, M. Ehara, K. Toyota, R. Fukuda, J. Hasegawa, M. Ishida, T. Nakajima, Y. Honda, Honda,O. Honda, H. Nakai, Nakai,T. Nakai, J. A. Montgomery, J. E. Peralta, F. Ogliaro, M. Bearpark, J. J. Heyd, E. Brothers, K. N. Kudin, V. N. Staroverov, R. Kobayashi, J. Normand, K. Raghavachari, A. Rendell, J. C. Burant, S. S. Iyengar, J. Tomasi, M. Cossi, N. Rega, J. M. Millam, M. Klene, J. E. Knox, J. B. Cross, V. Bakken, C. Adamo, J. Jaramillo, R. Gomperts, R. E. Stratmann, O. Yazyev, A. J. Austin, R. Cammi, C. Pomelli, J. W. Ochterski, R. L. Martin, K. Morokuma, V. G. Zakrzewski, G. A. Voth, P. Salvador, J. J. Dannenberg, S. Dapprich, A. P. Daniels, O. Farkas, J. B. Foresman, J. V. Ortiz, J. Cioslowski, D. J. Fox, *Gaussian 09, Gaussian, Inc.: Wallingford CT*, **2009**.
[75] M. J. Frisch, G. W. Trucks, H. B. Schlegel, G. E. Scuseria, M. A. Robb, J. R. Cheeseman, G. Scalmani, V. Barone, G. A. Petersson, H. Nakatsuji, X. Li, M. Caricato, A. V. Marenich, J. Bloino, B. G. Janesko, R. Gomperts, B. Mennucci, H. P. Hratchian, J. V. Ortiz, A. F. Izmaylov, J. L. Sonnenberg, D. Williams-Young, F. Ding, F. Lipparini, F. Egidi, J. Goings, B. Peng, A. Petrone, T. Henderson, D. Ranasinghe, V. G. Zakrzewski, J. Gao, N. Rega, G. Zheng, W. Liang, M. Hada, M. Ehara, K. Toyota, R. Fukuda, J. Hasegawa, M. Ishida, T. Nakajima, Y. Honda, O. Kitao, H. Nakai, T. Vreven, K. Throssell, J. Montgomery, J. A., J. E. Peralta, F.Ogliaro, M. J. Bearpark, J. J. Heyd, E. N. Brothers, K. N. Kudin, V. N. Staroverov, T. A. Keith, R. Kobayashi, J. Normand, K. Raghavachari, A. P. Rendell, J. C. Burant, S. S. Iyengar, J. Tomasi, M. Cossi, J. M. Millam, M. Klene, C. Adamo, R. Cammi, J. W. Ochterski, R. L. Martin, K. Morokuma, O. Farkas, J. B. Foresman, D. J. Fox, *Gaussian 16, Revision A.03; Gaussian, Inc.,: Wallingford CT*, **2016**.
[76] W. Kohn, A. D. Becke, R. G. Parr, *J. Phys. Chem.* **1996**, *100*, 12974–12980.
[77] C Lee, W. Yang, R. G. Parr, *Phys. Rev. B Condens. Matter* **1988**, *37*, 785–789.
[78] W. Yang, R. G. Parr, C. Lee, *Phys. Rev. A* **1986**, *34*, 4586–4590.
[79] T. H. Dunning, P. J. Hay, in *Methods Electron. Struct. Theory*, Springer, Boston, MA, **1977**, pp. 1–27.
[80] W. R. Wadt, P. J. Hay, *J. Chem. Phys.* **1985**, *82*, 284–298.
[81] P. J. Hay, W. R. Wadt, *J. Chem. Phys.* **1985**, *82*, 299–310.
[82] P. J. Hay, W. R. Wadt, *J. Chem. Phys.* **1985**, *82*, 270–283.
[83] S. I. Gorelsky, "AOMix, Software for Quantum Chemistry, Electron Population Analysis (Mulliken, Lowdin, CDA)," can be found under http://www.sg-chem.net/, **2013**.
[84] S. I. Gorelsky, A. B. P. Lever, *J. Organomet. Chem.* **2001**, *635*, 187–196.

Manuscript received: November 6, 2017
Version of record online: February 27, 2018